

# Introduction to Quantum-limited Parametric Amplification of Quantum Signals with Josephson Circuits

Michel Devoret<sup>a</sup>, and Ananda Roy<sup>a</sup>

<sup>a</sup>*Department of Applied Physics, Yale University, PO BOX 208284, New Haven, CT 06511*

---

## Abstract

This short and opinionated review starts with a concept of quantum signals at microwave frequencies and focuses on the principle of linear parametric amplification. The amplification process arises from the dispersive nonlinearity of Josephson junctions driven with appropriate tones. We discuss two defining characteristics of these amplifiers: the number of modes receiving the signal, idler and pump waves and the number of independent ports through which these waves enter into the circuit.

---

## 1. Introduction

Photons of microwave radiation in the band 3 – 12 GHz (25-100 mm wavelength) have an energy approximately  $10^5$  smaller than those of visible light. Yet, at a temperature  $2 \times 10^4$  smaller than room temperature, now routinely achievable with commercial dilution refrigerator, it is possible to detect and process signals whose energy is equivalent to that of single microwave photons [1]. There are three advantages of single photon microwave electronics when compared with quantum optics. First, signal envelopes with a relative bandwidth of few percent at carrier frequencies of a few GHz can be controlled with much greater relative precision than their equivalent at a few hundred of THz. This is because microwave generators have better short term stability than lasers, and also because microwave components are mechanically very stable, particularly when cooled, compared with traditional optical components. Second, on-chip circuitry of single-photon microwave electronics can be well in the lumped element regime and consequently, the control of spatial mode structure more easily achieved than in the optical domain. Finally, there exists a simple, robust, non-dissipative component, the Josephson tunnel junction, whose non-linearity can dominate over the linear characteristics of the circuit at the single photon level.

---

*Email addresses:* [michel.devoret@yale.edu](mailto:michel.devoret@yale.edu) (Michel Devoret), [ananda.roy@yale.edu](mailto:ananda.roy@yale.edu) (and Ananda Roy)

Many quantum signal processing functions have thus been realized, both digital and analog, and this short review will not attempt to describe all of them. We will concentrate here on analog Josephson amplifying devices pumped with one or several microwave tones. Only devices that demonstrate linear amplification with added noise at the level of the standard quantum limit [2] will be considered. These novel devices have taken the work pioneered by B. Yurke at Bell labs 30 years ago [3, 4] to the point where new original experiments can be performed successfully owing to Josephson amplifiers as the first link in the chain of measurements [5, 6].

The article is organized as follows. Sec. 2 is devoted to the in-depth description of signals that are considered quantum in the field of microwave electronics. We describe in Sec. 3 the important theoretical tool of the Quantum Langevin Equation with which the amplifier characteristics can be calculated, starting from the circuit Hamiltonian and the coupling parameters of its ports. Then, in the following Sec. 4, we will introduce the notion of effective parametric amplifier Hamiltonian. This will lead us to discuss the important distinction between the degenerate and non-degenerate amplifiers that arises from a fundamental difference in the degrees of freedom of the two devices. The practical implementation of amplifiers will be treated in Sec. 5. Finally, in Sec. 6, after a concluding summary, we will indicate the perspectives of the field.

## 2. Quantum electromagnetic signals propagating along transmission lines

Crudely speaking, quantum signals are electromagnetic excitations of a transmission line that involve only a few photons. The state of these excitations must display some degree of quantum purity for the signals to carry quantum information, which is the subject of interest in Josephson circuits. In this section, we provide the basic mathematical background for the concept of photon applied to microwave electromagnetic excitations [7, 8]. We start by considering an infinite transmission line, a one-dimensional electromagnetic medium characterized by a propagation velocity  $v_p$  and a characteristic impedance  $Z_c$ . A microwave coaxial line serves as the canonical example of such medium (see Fig. 1).

Position along the line is indexed by the real number  $x \in (-\infty, +\infty)$ . We suppose that the line is ideal, with both  $v_p$  and  $Z_c$  independent of frequency  $\omega$ . It is convenient to combine the voltage  $V(x, t)$  across the line with the current  $I(x, t)$  along the line in the  $+x$  direction into the so-called propagating wave amplitude

$$A^{\leftrightarrow}(x, t) = \frac{1}{2} \left[ \frac{1}{\sqrt{Z_c}} V(x, t) \pm \sqrt{Z_c} I(x, t) \right]. \quad (1)$$

Here, the superscript arrows refer to the two directions of propagation along the line. The wave amplitude, whose dimension is  $[\text{watt}]^{1/2}$ , is such that its square is the energy flux of waves traveling in the direction indicated by the arrow. This interpretation is justified by the formula giving the total energy flux at

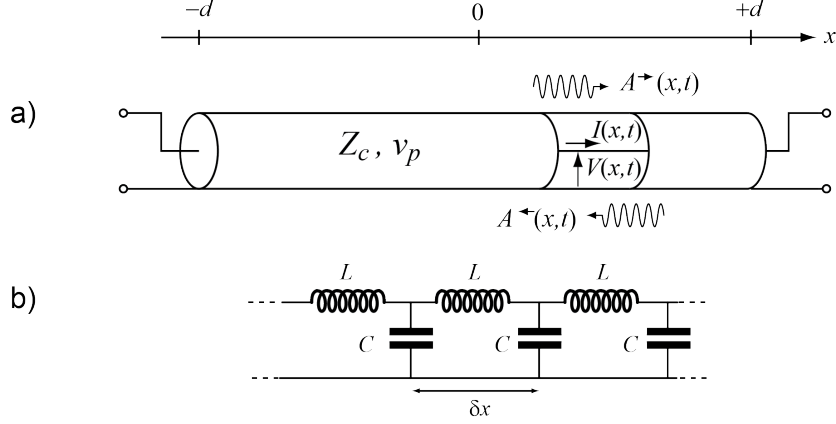


Figure 1: (a) Electromagnetic transmission line implemented as a coaxial cable. The parameter  $x$  denotes the position along the line,  $I$  denotes the current along the line in the positive direction and  $V$  the voltage between the inner and outer conductors. The characteristic impedance and the propagation velocity are denoted by  $Z_c$  and  $v_p$ , respectively. The line has a continuous density of modes in the limit where its length  $2d \rightarrow \infty$ . In (b), a ladder circuit model with cell dimension  $\delta x$  models the infinite transmission line. Its capacitance and inductance per unit length are given by  $L_\ell = L/\delta x$  and  $C_\ell = C/\delta x$ , respectively. In the limit where the signal frequency  $\omega$  is small compared to  $1/\sqrt{L_\ell C_\ell}$ ,  $Z_c = \sqrt{L/C}$  and  $v_p = 1/\sqrt{L_\ell C_\ell}$ .

time  $t$  crossing the location  $x$ , which is the equivalent of the Poynting vector for a one-dimensional medium:

$$P(x, t) = |A^\rightarrow(x, t)|^2 - |A^\leftarrow(x, t)|^2 = V(x, t) I(x, t). \quad (2)$$

Because the voltage and current obey the equivalent of Maxwell's equations

$$\frac{\partial V}{\partial x} = -L_\ell \frac{\partial I}{\partial t}, \quad (3)$$

$$\frac{\partial I}{\partial x} = -C_\ell \frac{\partial V}{\partial t}, \quad (4)$$

where  $(L_\ell C_\ell)^{-1/2} = v_p$  and  $(L_\ell/C_\ell)^{1/2} = Z_c$ , the wave amplitude has the space-time translation invariance properties of traveling electromagnetic waves

$$A^\pm(x, t) = A^\pm(0, t \mp x/v_p) = A^\pm(x \mp v_p t, 0). \quad (5)$$

This shows that the entire field in the line is completely described by the left-moving and right-moving components at time  $t = 0$  for all position  $x$ . Equivalently, the field is described by the left-moving and right-moving components at  $x = 0$  for all times  $t$ . We now introduce the wave amplitude operator, which describes the electromagnetic field of the line quantum-mechanically

$$A^\pm(x, t) \rightarrow \mathbf{A}^\pm(x). \quad (6)$$

Instead of a space index, we can give the wave amplitude operator a time index, which is trivially deduced from the space index

$$\mathbf{A}^{\rightleftharpoons}(x) \Longleftrightarrow \mathbf{A}^{\rightleftharpoons}\left(t = \pm \frac{x}{v_p}\right). \quad (7)$$

The commutation properties of the wave amplitude operator, which is hermitian, are rather complex. The route to the mathematical introduction of the microwave photon is easier if we first make a detour through Fourier space. We define

$$\mathbf{A}^{\rightleftharpoons}[\omega] = \frac{1}{\sqrt{2\pi}} \int_{-\infty}^{+\infty} dt e^{i\omega t} \mathbf{A}^{\rightleftharpoons}(t), \quad (8)$$

which describes the wave amplitude operator in the frequency domain (no real time dynamics is considered here, as the time index is equivalent to a space index and the reciprocal space equivalent to the wave vector space). We now introduce field ladder operators

$$\mathbf{a}^l[\omega] = \frac{1}{\sqrt{\hbar|\omega|/2}} \mathbf{A}^l[\omega], \quad (9)$$

where the superscripts  $l = \pm 1$  denote the direction of propagation  $\rightarrow$  or  $\leftarrow$  (we will generalize later the index  $l$  to include the line number, i.e. spatial mode number). The field ladder operators  $\mathbf{a}^l[\omega]$  have commutation relations bearing a marked resemblance to the ladder operators of a set of standing wave harmonic oscillators

$$[\mathbf{a}^{l_1}[\omega_1], \mathbf{a}^{l_2}[\omega_2]] = \text{sgn}(\omega_1 - \omega_2) \delta(\omega_1 + \omega_2) \delta_{l_1, l_2}. \quad (10)$$

This is somewhat clearer when we take into account that

$$\mathbf{a}^l[\omega]^\dagger = \mathbf{a}^l[-\omega]. \quad (11)$$

Yet, these operators do not correspond directly to the traveling photon ladder operators. We go back in the time domain and introduce

$$\mathbf{a}^l(t) = \frac{1}{\sqrt{2\pi}} \int_{-\infty}^{+\infty} d\omega e^{-i\omega t} \mathbf{a}^l[\omega] = \tilde{\mathbf{a}}^l(t) + \tilde{\mathbf{a}}^l(t)^\dagger, \quad (12)$$

$$\tilde{\mathbf{a}}^l(t) = \frac{1}{\sqrt{2\pi}} \int_0^{+\infty} d\omega e^{-i\omega t} \mathbf{a}^l[\omega], \quad (13)$$

$$\tilde{\mathbf{a}}^l(t)^\dagger = \frac{1}{\sqrt{2\pi}} \int_{-\infty}^0 d\omega e^{-i\omega t} \mathbf{a}^l[\omega]. \quad (14)$$

It is important to note that with our notations  $\tilde{\mathbf{a}}^l(t)$  is NOT the inverse Fourier transform of  $\mathbf{a}^l[\omega]$ , since it involves only positive frequencies  $\omega$ . The inverse Fourier transform of  $\mathbf{a}^l[\omega]$  is  $\mathbf{a}^l(t)$ , which is a *hermitian* operator. The dimension of the operators  $\tilde{\mathbf{a}}^l(t)$  is the inverse square root of time and it would

be tempting to interpret them as photon flux amplitudes. However, in the time domain, the commutation relations of the field ladder operators do not take the usual bosonic form of a scalar field

$$\begin{aligned} \left[ \tilde{\mathbf{a}}^l(t_1), \mathbf{a}^l(t_2)^\dagger \right] &= \frac{1}{2\pi} \left[ \int_0^{+\infty} d\omega_1 e^{-i\omega_1 t_1} \mathbf{a}[\omega_1], \int_{-\infty}^0 d\omega_2 e^{-i\omega_2 t_2} \mathbf{a}[\omega_2] \right] \\ &= \frac{1}{2} \delta(t_1 - t_2) + \frac{i}{2\pi} \text{p.p.} \left( \frac{1}{t_1 - t_2} \right). \end{aligned} \quad (15)$$

On the other hand,

$$[\mathbf{a}^{l_1}(t_1), \mathbf{a}^{l_2}(t_2)] = \delta(t_1 - t_2) \delta_{l_1, l_2}. \quad (16)$$

In order to properly define the photons of the line, one needs to introduce an orthonormal signal basis consisting of “first-quantization” wavelets  $w_{mp}^l(t)$  such that

$$\int_{-\infty}^{+\infty} dt w_{m_1 p_1}^{l_1}(t) w_{m_2 p_2}^{l_2}(t)^* = \delta_{m_1, m_2} \delta_{p_1, p_2} \delta_{l_1, l_2}, \quad (17)$$

$$w_{mp}^l(t)^* = w_{-mp}^l(t), \quad (18)$$

$$\sum_{m=-\infty}^{+\infty} \sum_{p=-\infty}^{+\infty} w_{mp}^l(t_1) w_{-mp}^l(t_2) = \delta(t_1 - t_2). \quad (19)$$

The pair of indices  $(|m|, p) \in \mathbb{N}^+ \times \mathbb{Z}$  defines a propagating temporal mode of the line, and the combined amplitudes of the two corresponding wavelets can be seen as an elementary degree of freedom of the field. There are two conjugate wavelets per mode since the phase space of each mode is bi-dimensional.

It is often convenient, but not necessary, to request that the support of  $w_{mp}^l[\omega]$ , the Fourier transform of  $w_{mp}^l(t)$ , is entirely contained in the positive frequency sector if  $m > 0$  and in the negative frequency sector if  $m < 0$ .

$$w_{mp}^l[\omega] = w_{mp}^l[\omega] \Theta(\omega) \quad \text{if} \quad m > 0, \quad (20)$$

$$w_{mp}^l[\omega] = w_{mp}^l[\omega] \Theta(-\omega) \quad \text{if} \quad m < 0. \quad (21)$$

In these last expressions,  $\Theta(\omega)$  is the Heaviside function<sup>1</sup>.

This complete wavelet basis is a purely classical signal processing concept and its existence solely results from the property of the signals to be square-integrable functions. Any continuous signal  $f(t)$  such that  $\int_{-\infty}^{+\infty} |f(t)|^2 dt < \infty$  can indeed be decomposed into a countable infinite number of elementary signals

$$f(t) = \sum_{m=-\infty}^{+\infty} \sum_{p=-\infty}^{+\infty} f_{mp} w_{mp}(t), \quad (22)$$

$$f_{mp} = \int_{-\infty}^{+\infty} dt w_{mp}(t) f(t). \quad (23)$$

---

<sup>1</sup>The index value  $m = 0$  corresponds to special wavelets that have to be treated separately.

A common example of such a wavelet is the Shannon wavelet

$$\mathfrak{w}_{mp}(t) = 2\sqrt{\frac{\tau}{2\pi}} \frac{\sin\left(\frac{\pi}{\tau}(t - p\tau)\right)}{t} e^{i2\pi mt/\tau} \quad (24)$$

whose Fourier transform is

$$\mathfrak{w}_{mp}[\omega] = \sqrt{\frac{\tau}{2\pi}} 1_{\frac{2\pi}{\tau}(m-1/2), \frac{2\pi}{\tau}(m+1/2)}(\omega) e^{ip\omega\tau}, \quad (25)$$

where  $1_{x_1, x_2}(x)$  is the indicator function which is 0 everywhere except in the interval  $[x_1, x_2]$ , where its value is unity. Many other useful bases, involving more continuous wavelets, exist [9]. In the above example, the center frequency and time location of the wavelet is  $2\pi m/\tau$  and  $p\tau$ , respectively (in order to form a complete basis, the pitch in frequency  $\Delta\omega$  and pitch in time  $\Delta t$  of the wavelet basis has to satisfy  $\Delta\omega \cdot \Delta t \leq 2\pi$ ).

The discreteness of the signal component indices is the justification for the term “first-quantization” and no quantum mechanics is involved here since all functions are at this stage c-number valued. Second-quantization intervenes when we define the discrete ladder field operators, with indices  $m > 0$  and  $p$

$$\psi_{mp}^l = \int_{-\infty}^{+\infty} d\tau w_{mp}^l(\tau) \mathbf{a}^l(\tau), \quad (26)$$

$$\psi_{-mp}^l = \psi_{mp}^{l\dagger}. \quad (27)$$

We introduce the short-hand  $\mu = (l, |m|, p)$  as the index of the spatio-temporal mode, also called the flying oscillator. The photon-number operator is given by:

$$\mathbf{n}_\mu = \psi_\mu^\dagger \psi_\mu \quad (28)$$

and the discrete ladder operators  $\psi_\mu$  satisfy the same commutation relation as standing mode ladder operators:

$$\begin{aligned} [\psi_{\mu_1}, \psi_{\mu_2}^\dagger] &= \int_{-\infty}^{+\infty} \int_{-\infty}^{+\infty} dt_1 dt_2 w_{m_1 p_1}^{l_1}(t_1) w_{m_2 p_2}^{l_2}(t_2)^* [\mathbf{a}^{l_1}(t_1), \mathbf{a}^{l_2}(t_2)] \\ &= \delta_{\mu_1, \mu_2}. \end{aligned} \quad (29)$$

An important remark can be made: if the photon amplitude operator  $\psi_\mu$  is non-hermitian, this is only because its first quantization component  $w_{mp}^l(\tau)$  is complex. Its second quantization component  $\mathbf{a}^l(\tau)$  is an hermitian operator. It is also important to note that, in general, the frequency of a photon is ill-defined, in contrast with what could be inferred from elementary introductions to quantum mechanics. This feature happens as soon as the duration of the wavelet corresponding to that particular photon is not very long compared with the inverse of the wavelet center frequency. Thus the concept of photon for a propagating signal has to be clearly distinguished from an energy quantum. A

propagating photon is an elementary excitation of the field carrying a quantum of action, and corresponds to a field wavefunction orthogonal to the vacuum.

$$|\Psi_{1\mu}\rangle = \psi_\mu^\dagger |\text{vac}\rangle, \quad (30)$$

$$\langle \text{vac} | \Psi_{1\mu} \rangle = 0. \quad (31)$$

A wavelet can contain several photons in mode  $\mu$

$$|\Psi_{n\mu}\rangle = \frac{1}{\sqrt{n!}} (\psi_\mu^\dagger)^n |\text{vac}\rangle \quad (32)$$

and each multi-photon state (Fock state) is orthogonal to the others

$$\langle \Psi_{n_2\mu} | \Psi_{n_1\mu} \rangle = \delta_{n_1 n_2}. \quad (33)$$

Several modes can simultaneously be excited

$$|\Psi_{n_1, \mu_1; n_2, \mu_2; n_3, \mu_3; \dots}\rangle = \frac{1}{\sqrt{n_1!}} (\psi_{\mu_1}^\dagger)^{n_1} \frac{1}{\sqrt{n_2!}} (\psi_{\mu_2}^\dagger)^{n_2} \frac{1}{\sqrt{n_3!}} (\psi_{\mu_3}^\dagger)^{n_3} \dots |\text{vac}\rangle. \quad (34)$$

The sequence of indices  $\sigma = (n_1, \mu_1; n_2, \mu_2; n_3, \mu_3; \dots)$  is a mode photon occupancy configuration. Finally, the most general wavefunction of the field of the transmission line(s) is a superposition of all field photon configurations in all the spatio-temporal modes of the line(s):

$$|\Psi\rangle = \sum_{\sigma} C_{\sigma} |\Psi_{\sigma}\rangle. \quad (35)$$

There are exponentially many more quantum coefficients  $C_{\sigma}$  than the classical coefficients  $f_{\mu}$  in Eq. (23)! And it is also important to understand that a state with a well defined number of photons in a certain wavelet basis can be fully entangled in another basis.

A wavelet can also support a so-called coherent state instead of a well defined number of photons:

$$|\alpha_{\mu}\rangle = e^{-|\alpha_{\mu}|^2/2} \sum_n \frac{\alpha_{\mu}^{n/2}}{\sqrt{n!}} |\Psi_{n\mu}\rangle, \quad (36)$$

$$= e^{-|\alpha_{\mu}|^2/2} e^{\alpha_{\mu} \psi_{\mu}^\dagger} |\text{vac}\rangle, \quad (37)$$

and if all wavelets are in a coherent state, we obtain a coherent field state

$$|\Psi_{\{\alpha\}}\rangle = \prod_{\mu} |\alpha_{\mu}\rangle \quad (38)$$

$$= e^{-\sum_{\mu} (|\alpha_{\mu}|^2/2 - \alpha_{\mu} \psi_{\mu}^\dagger)} |\text{vac}\rangle. \quad (39)$$

Thus, the set of complex coefficients  $\alpha_{\mu}$  plays the role of the coefficients  $f_{\mu}$  in Eq. (23). Somewhat surprisingly, this property of being a coherent state remains

true in *every* wavelet basis (as can be inferred from the quadratic form in the exponent of Eq. [39]).

The state of the line is in general not pure and must be described by a density matrix  $\rho_{\sigma\sigma'}$ . This ultimate quantum field description tool leads to the important notion of information contained in the signal.

In general, in quantum mechanics, we can define for a system with a finite-dimension Hilbert space, the Shannon–Von Neumann entropy

$$S = -\text{tr} \rho \ln \rho. \quad (40)$$

The information contained in the system is then straightforwardly computed as

$$\mathcal{I} = S(\rho_{\text{mix}}) - S(\rho), \quad (41)$$

where  $\rho_{\text{mix}}$  is the fully mixed state in which all basis states are equiprobable, with no off-diagonal correlations. The extension of these ideas to a transmission line on which a signal propagates is not trivial since the number of temporal modes is infinite and each temporal mode has a Hilbert space with infinite dimensionality. Some constraints need to be provided, for instance a fixed total energy for both  $\rho$  and  $\rho_{\text{mix}}$ . We can also, in another instance, fix the maximum number of excitation in each temporal mode. Supposing that the maximum number of excitations is unity in the domain  $(|m|, p) \in \{1, 2, \dots, M\} \otimes \{-P, \dots, +P\}$  and that other modes are in the vacuum state, then, for a state of the line characterized by an average photon number  $\langle n_{|m|p} \rangle$  per mode

$$\mathcal{I} = \sum_{m=1}^M \sum_{p=-P}^P \mathcal{I}_b(\langle n_{|m|p} \rangle - 1/2), \quad (42)$$

where  $\mathcal{I}_b(\langle X \rangle)$  the information contained in a stochastic binary variable  $X = \pm 1$ :

$$\mathcal{I}_b(x) = \log_2 \left[ \sqrt{1-x^2} \left( \frac{1+|x|}{1-|x|} \right)^{\frac{|x|}{2}} \right]. \quad (43)$$

We refer the reader to [10] for a more complete description of the information carried by quantum signals.

### 3. Quantum Langevin Equation

The main role of the previous section was to introduce the concept of quantum electromagnetic fields propagating along a transmission line at microwave frequencies. The elementary excitations of these fields, microwave photons, can be seen as the carriers of the information transmitted by the propagating field. An amplifier is a particular case of a signal processing device. In general, a signal processing device is a lumped element circuit that is connected to two semi-infinite transmission lines [see Fig. 2 (a)]. It receives from the input line the propagating signal carrying the information to be processed and re-emits in



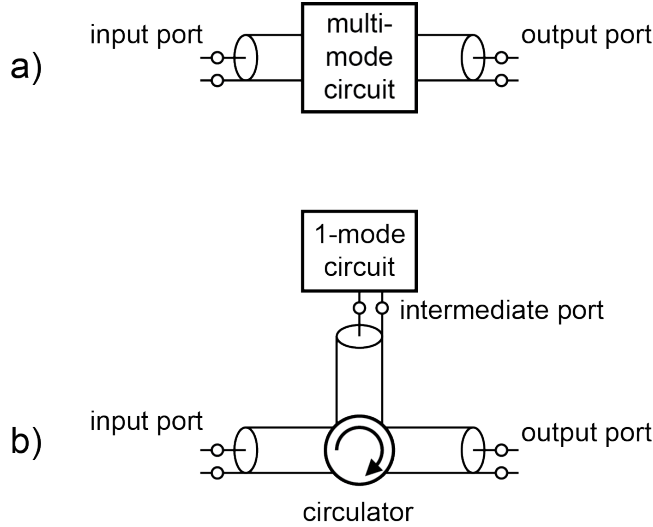


Figure 2: Circuit modes and ports: a) We are interested in quantum signal processing circuits in lumped element regime, which possess in general several standing modes. Input lines and output lines are attached to ports. In the simplest case b), a one-mode circuit communicates with the outside through only one port. An ideal circulator separates the input from the output.

the output line another signal carrying the result of the information processing. A crucial ingredient, in the description of the mapping of the input signal into the output signal, is the coupling between the circuit, which houses standing electromagnetic modes, and the transmission lines, which support propagating modes. This coupling is dealt with theoretically through the Quantum Langevin Equation. We will first consider its simplest version in which a lumped element circuit with only one electromagnetic mode is coupled to only one semi-infinite transmission line [Fig. 2 (b)].

In this so-called one-mode, one-port configuration, the signal processing occurs as a transformation of the incoming wave into the reflected outgoing wave. However, in order to utilize the action of the one-mode, one-port circuit, a non-reciprocal linear device called a circulator has to be added in order to separate the incoming and outgoing waves into two independent transmission lines [Fig. 2 (b)]. This circuit configuration also provides a way to model directional, through amplifiers [11]. We can leave the modeling of the circulator aside for the moment (it is a 3-port device), and just write the equation linking the quantum amplitude  $\mathbf{a}$  of the circuit, satisfying  $[\mathbf{a}, \mathbf{a}^\dagger] = 1$ , to the incoming quantum field amplitude of the line  $\mathbf{a}^{\text{in}}(t)$  at the unique port (this is the generic name of the interface between a semi-infinite transmission line and a lumped element circuit)

$$\frac{d\mathbf{a}}{dt} \underset{\substack{\text{Markov} \\ \text{RWA}}}{=} = \frac{i}{\hbar} [\mathbf{H}, \mathbf{a}] - \frac{\kappa}{2} \mathbf{a} + \sqrt{\kappa} \mathbf{a}^{\text{in}}(t), \quad (44)$$

where  $\mathbf{a}^{\text{in}}$  is the traveling photon amplitude defined in the last section (Eq. (12)), the superscript “in” referring to the sense of propagation coming into the circuit. The equation (44) is a special case of the Quantum Langevin Equation (QLE) [7] and its right handside has three terms. The first term corresponds to that of the usual Heisenberg equation of motion for an operator in quantum mechanics, in which  $\mathbf{H}$  is the Hamiltonian of the circuit, written as a function of the conjugate ladder operators  $\mathbf{a}$  and  $\mathbf{a}^\dagger$ . The circuit can be arbitrarily non-linear and thus  $\mathbf{H}$  will be in general more sophisticated than the simple quadratic term  $\hbar\omega_a \mathbf{a}^\dagger \mathbf{a}$  of the quantum harmonic oscillator. Next, the second term is a damping term specific to both the open nature of the system, and the linear coupling between the circuit and the transmission line. Its remarkable simple form requires two assumptions: i) The so-called Markov approximation which considers that the coupling of the system with the environment is “ohmic”: the density of modes of the environment can be considered white across the set of circuit transition frequencies, as in an ideal resistance. ii) The coupling is also supposed to be weak in the sense that  $\kappa$  is much smaller than any transition frequency between the energy levels of the lumped circuit. This is the so-called Rotating Wave Approximation (RWA). Finally, the third and last term on the right handside of the Quantum Langevin Equation describes the role of the incoming field as a drive for the circuit. It represents the counterpart of the energy loss modeled by the second term. Although approximations are made, the equation respects the important commutation relation of the ladder operators:

$$[\mathbf{a}(t), \mathbf{a}(t)^\dagger] = 1 \quad (45)$$

at all times  $t$ .

The incoming driving field has in general three components which are treated on equal footing by the QLE: i) the deterministic signal to be processed, ii) thermal or parasitic noise accompanying the information-carrying signal, and iii) quantum noise, or, in other words, the zero-point fluctuations of the field of the semi-infinite transmission line. The inclusion of this last component is implemented implicitly in that the Quantum Langevin Equation is an operator equation, in contrast with the Classical Langevin Equation which is just a differential equation for a c-number function, albeit stochastic. Note that the coefficient  $\sqrt{\kappa}$  in front of the propagating field amplitude embodies single-handedly the fluctuation-dissipation theorem: the rate at which energy is radiated away from the circuit (the coefficient  $\kappa$  of the second term) has to be tightly linked to the coupling constant with which random radiation – emitted from the black body that the line plays the role of – corrupt the purity of the state of the circuit. If one wonders why  $\kappa$  appears under a square root in this coupling coefficient, one just needs to remember that while  $\mathbf{a}$  is a dimensionless standing photon number

amplitude,  $\mathbf{a}^{\text{in}}(t)$  is the dimensioned amplitude corresponding to a photon flux. Consequently, when the semi-infinite line is in thermal equilibrium (input signal is only black-body noise with temperature  $T$ ), the following relation involving the anticommutator  $\{\square, \square\}$  holds

$$\langle \{ \mathbf{a}^{\text{in}}[\omega_1], \mathbf{a}^{\text{in}}[\omega_2] \} \rangle_T = \coth \frac{\hbar(\omega_1 - \omega_2)}{4k_B T} \delta(\omega_1 + \omega_2), \quad (46)$$

where  $k_B$  is Boltzmann constant,  $\{\mathbf{A}, \mathbf{B}\} = \mathbf{AB} + \mathbf{BA}$  and  $\langle \dots \rangle_T$  the average in the thermal state. Given an operating temperature around 20 mK, this expression shows that the quantum fluctuations become fully dominant over thermal fluctuations at frequencies above a GHz.

In principle, one can integrate the QLE and express the circuit variable  $\mathbf{a}(t)$  in terms of the incoming field  $\mathbf{a}^{\text{in}}(t)$ . The output field can be obtained from the Input-Output Equation

$$\sqrt{\kappa} \mathbf{a} = \mathbf{a}^{\text{in}}(t) + \mathbf{a}^{\text{out}}(t). \quad (47)$$

Again, the appearance of the simple coefficient  $\sqrt{\kappa}$  in this relation results from the Markov approximation.

When the circuit is a simple harmonic oscillator  $H = \hbar\omega_0 \mathbf{a}^\dagger \mathbf{a}$ , see Fig. 3, the elimination of  $\mathbf{a}$  between input and output can be carried out fully at the analytical level and one obtains

$$\left( \frac{d}{dt} + i\omega_0 + \kappa/2 \right) \mathbf{a}^{\text{out}}(t) = - \left( \frac{d}{dt} + i\omega_0 - \kappa/2 \right) \mathbf{a}^{\text{in}}(t). \quad (48)$$

Going to the Fourier domain, one obtains the reflection coefficient  $r(\omega)$

$$\mathbf{a}^{\text{out}}[\omega] = r(\omega) \mathbf{a}^{\text{in}}[\omega], \quad (49)$$

$$r_{\text{RWA}}(\omega) = - \frac{\omega - \omega_0 - i\kappa/2}{\omega - \omega_0 + i\kappa/2}. \quad (50)$$

The causality property of the circuit, which expresses the fact that it cannot produce a response *before* being submitted to a stimulus, is implemented here by the analytic property of the complex function  $r_{\text{RWA}}(\omega)$ : its pole is in the lower half complex plane while its zero is in the upper half. On the other hand, the fact that the reflection coefficient has only one pole instead of a pair is an artefact of RWA. As a matter of fact, when the circuit is linear as in Fig. 3, one can compute exactly the reflection coefficient using a more elaborate form of QLE without RWA, while keeping the Markov approximation. One then obtains the expression possessing the necessary pair of poles with values  $\omega_{\pm} = (-i\kappa \pm \sqrt{-\kappa^2 - 4\omega_0^2})/2$ :

$$r(\omega) = - \frac{\omega^2 - \omega_0^2 - i\kappa\omega}{\omega^2 - \omega_0^2 + i\kappa\omega}. \quad (51)$$

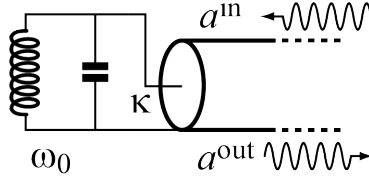


Figure 3: Schematic of the circuit corresponding to a 1-port 1-mode passive linear device.

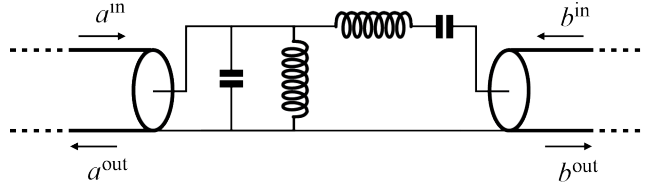


Figure 4: Example of a two-mode, two-port circuit in which care must be taken in the amplitude factors of the Quantum Langevin Equation.

It is easy to see that in this last equation,  $r(\omega)$  reduces to the single pole expression  $r_{\text{RWA}}(\omega)$  when  $\omega$  is such that  $|1 - \omega/\omega_0| \ll 1$  and in the underdamped limit  $\kappa/\omega_0 \ll 1$ .

Continuing to work in the framework of both RWA and the Markov approximation, one can easily deal with more than one circuit mode and more than one semi-infinite line. Denoting by  $M$  the circuit standing mode index and  $P$  the port index, one obtains the multi-mode, multi-port generalized QLE:

$$\frac{d}{dt} \mathbf{a}_M = \frac{i}{\hbar} [\mathbf{H}, \mathbf{a}_M] + \sum_P \left[ -\frac{\kappa_{MP}}{2} \mathbf{a}_M + \varepsilon_{MP} \sqrt{\kappa_{MP}} \mathbf{a}_P^{\text{in}}(t) \right]. \quad (52)$$

Apart from a simple extension of the number of variables, this new equation contains the rectangular matrix  $\varepsilon_{MP}$  whose complex coefficients are such that  $|\varepsilon_{MP}| = 1$ . This matrix can be computed from the details of the coupling of the lines to particular elements of the circuit (capacitances or inductances, series or parallel connections). A simple example of a situation where the  $\varepsilon_{MP}$  cannot be set to unity by a re-definition of the mode amplitude  $\mathbf{a}_M$  is presented in Fig. 4. The general Input-Output Equation takes the form

$$\mathbf{a}_M = \sum_P \frac{1}{\sqrt{\kappa_{MP}}} [\varepsilon_{MP} \mathbf{a}_M^{\text{in}}(t) + \varepsilon_{MP}^{-1} \mathbf{a}_P^{\text{out}}(t)]. \quad (53)$$

#### 4. Model amplifiers

We have in the previous section introduced the Quantum Langevin Equation and the Input-Output Equation which together allow, at least formally, to

compute how a given circuit processes signals propagating on transmission lines. We have treated the simplest case of a 1-mode, 1-port circuit implementing an harmonic oscillator circuit. However, the understanding of amplifiers starts by considering necessarily a generalization of the simple harmonic case, namely that of an effective, time-dependent quadratic Hamiltonian for the circuit. We defer to the next section the discussion of how these Hamiltonians emerge in practice from damped-driven non-linear systems. We will address first the question of how an amplification function can arise from such emergent effective quadratic form. Thus, let us consider the time-dependent effective quadratic Hamiltonian

$$\frac{\mathbf{H}}{\hbar} = \sum_m \omega_m \mathbf{a}_m^\dagger \mathbf{a}_m + i \sum_{m \leq p} g_{mp}^{\text{eff}} \left( \mathbf{a}_m \mathbf{a}_p e^{i(\Omega_{mp}t + \theta_{mp})} - h.c. \right) + \text{neglected terms}, \quad (54)$$

where  $m$  and  $p$  are circuit mode indices, and where the real, positive parameters  $\omega_m$  and  $g_{ml}^{\text{eff}}$  are in general functions of elementary parameters of the circuit combined with the values of time-dependent driving fields imposed from the outside and treated classically. These driving fields excite the circuit, thus providing energy for the amplification process and are often nicknamed “pumps”. We suppose that there are ports that couple the modes  $m$  to the outside world. In the case of one port per mode, this coupling is described by constants  $\kappa_m$ . The phase factors  $e^{i\theta_{mp}}$  depend on the details of the excitation, while the drive frequencies  $\Omega_{mp}$  are in the vicinity of  $\omega_m + \omega_p$  (or sometimes  $|\omega_m - \omega_p|$ , but we will not deal with this case here). By vicinity, we mean within the bandwidth determined by the port coupling constants:  $|\Omega_{mp} - \omega_m - \omega_p| \leq \kappa_m \kappa_p / (\kappa_m + \kappa_p)$ . Here, we will limit ourselves to two elementary cases: i) the simple two-port, 2-mode, non-degenerate parametric amplifier with Hamiltonian

$$\frac{\mathbf{H}^{\text{NDPA}}}{\hbar} = \omega_a \mathbf{a}^\dagger \mathbf{a} + \omega_b \mathbf{b}^\dagger \mathbf{b} + i g_{ab} \left( \mathbf{a} \mathbf{b} e^{i(\Omega_{ab}t + \theta)} - h.c. \right) \quad (55)$$

and port coupling constants  $\kappa_a$  and  $\kappa_b$ , and ii) the simple one-port, 1-mode, degenerate parametric amplifier with Hamiltonian

$$\frac{\mathbf{H}^{\text{DPA}}}{\hbar} = \omega_a \mathbf{a}^\dagger \mathbf{a} + i g_{aa} \left( \mathbf{a}^2 e^{i(\Omega_{aa}t + \theta)} - h.c. \right). \quad (56)$$

In this case, there is a single port coupling constant  $\kappa_a$ . The frequency landscapes corresponding to the two cases are represented schematically on Fig. 5.

From the Langevin Equation [Eq. (44)] and the Input-Output Equation [Eq. (47)] of the last section, we obtain for non-degenerate case (i) the pair of equations:

$$\begin{aligned} F(\omega_a, \kappa_a) \mathbf{a}^{\text{out}} + g_{ab} e^{-i(\Omega_{ab}t + \theta)} \mathbf{b}^{\text{out}\dagger} &= -F(\omega_a, -\kappa_a) \mathbf{a}^{\text{in}} - g_{ab} e^{-i(\Omega_{ab}t + \theta)} \mathbf{b}^{\text{in}\dagger}, \\ F(\omega_b, \kappa_b) \mathbf{b}^{\text{out}} + g_{ab} e^{-i(\Omega_{ab}t + \theta)} \mathbf{a}^{\text{out}\dagger} &= -F(\omega_b, -\kappa_b) \mathbf{b}^{\text{in}} - g_{ab} e^{-i(\Omega_{ab}t + \theta)} \mathbf{a}^{\text{in}\dagger}, \end{aligned}$$

where  $F(\omega, \kappa) = d/dt + i\omega + \kappa/2$ . For degenerate case (ii) there is only one equation:

$$F(\omega_a, \kappa_a) \mathbf{a}^{\text{out}} + 2g_{aa} e^{-i(\Omega_{aa}t + \theta)} \mathbf{a}^{\text{out}\dagger} = -F(\omega_a, -\kappa_a) \mathbf{a}^{\text{in}} - 2g_{aa} e^{-i(\Omega_{aa}t + \theta)} \mathbf{a}^{\text{in}\dagger}.$$

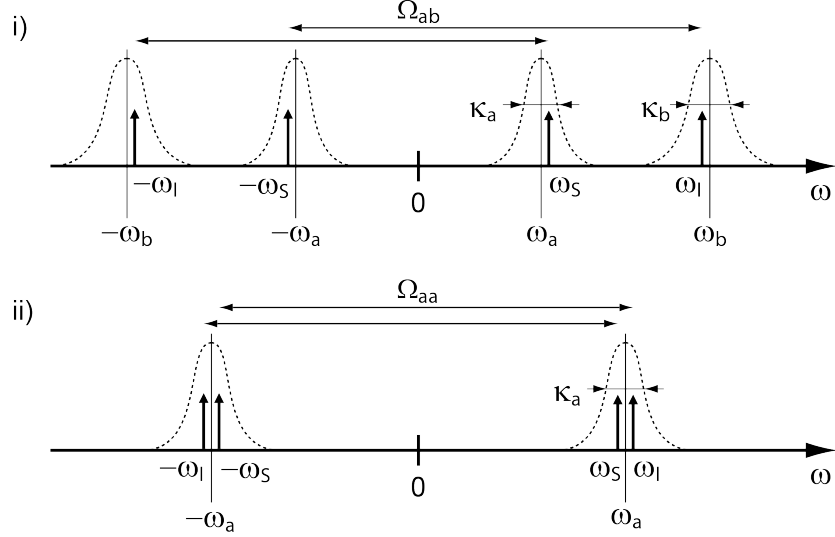


Figure 5: Frequency landscape for the non-degenerate (i) and degenerate (ii) parametric amplifiers. The dashed lines corresponds to response curves of each mode, as measured by a probe tone injected in the circuit elements of the mode. The vertical arrows correspond to the spectral densities of the signal and the idler tones arriving in the circuit through its ports. The horizontal arrows denote the frequency translations between signal and idler operated by the parametrical modulation induced by the pump tone.

Going to the Fourier domain and solving for outgoing waves as a function of the incoming waves we find for case (i)

$$\begin{bmatrix} \mathbf{a}^{\text{out}}[+\omega_S] \\ \mathbf{a}^{\text{out}}[-\omega_S] \\ \mathbf{b}^{\text{out}}[+\omega_I] \\ \mathbf{b}^{\text{out}}[-\omega_I] \end{bmatrix} = \begin{bmatrix} r_{SS} & 0 & 0 & s_{SI} \\ 0 & r_{SS}^* & s_{SI}^* & 0 \\ 0 & s_{IS}^* & r_{II}^* & 0 \\ s_{IS} & 0 & 0 & r_{II} \end{bmatrix} \begin{bmatrix} \mathbf{a}^{\text{in}}[+\omega_S] \\ \mathbf{a}^{\text{in}}[-\omega_S] \\ \mathbf{b}^{\text{in}}[+\omega_I] \\ \mathbf{b}^{\text{in}}[-\omega_I] \end{bmatrix}, \quad (57)$$

where  $\omega_S, \omega_I$  are the two signal and image (or idler) frequencies, respectively, linked precisely by  $\omega_S + \omega_I = \Omega_{ab}$ . Unlike in the case of simple harmonic circuits, an input signal at one frequency can here be processed into an output signal at another frequency. There is also a change in sign of the frequency in this process, which is called phase conjugation, and this is why we represent the scattering by a  $4 \times 4$  matrix. That matrix can be separated into two blocks related by the simple complex conjugation relating Fourier coefficients with opposite frequencies, a mathematical operation independent of the physical phenomenon of phase conjugation. Phase conjugation manifests itself practically in the following manner: if one advances the phase of the input signal by a given quantity, the phase of the conjugated output signal becomes retarded by the

same quantity. The elements of the scattering matrix are given by

$$r_{SS} = \frac{\chi_a^{-1}(\omega_S)^* \chi_b^{-1}(\omega_I)^* + \rho_{ab}^2}{\chi_a^{-1}(\omega_S) \chi_b^{-1}(\omega_I)^* - \rho_{ab}^2}, \quad (58)$$

$$r_{II} = \frac{\chi_a^{-1}(\omega_S) \chi_b^{-1}(\omega_I) + \rho_{ab}^2}{\chi_a^{-1}(\omega_S) \chi_b^{-1}(\omega_I)^* - \rho_{ab}^2}, \quad (59)$$

$$s_{SI} = \frac{2\rho_{ab}e^{-i\theta}}{\chi_a^{-1}(\omega_S) \chi_b^{-1}(\omega_I)^* - \rho_{ab}^2}, \quad (60)$$

$$s_{IS} = \frac{2\rho_{ab}e^{i\theta}}{\chi_a^{-1}(\omega_S) \chi_b^{-1}(\omega_I)^* - \rho_{ab}^2}. \quad (61)$$

These expressions contain two ingredients: the single mode bare susceptibilities  $\chi$ , which are given by

$$\chi_m(\omega) = \frac{1}{1 - 2i(\omega - \omega_m)/\kappa_m} \quad (62)$$

and the reduced effective mode coupling given by

$$\rho_{ab} = \frac{2g_{ab}}{\sqrt{\kappa_a \kappa_b}}. \quad (63)$$

Its modulus squared is often called the mode cooperativity. When the drive tone of the amplifier is optimally tuned  $\Omega_{ab} = \omega_a + \omega_b$  and when monochromatic input signals are on resonance with their corresponding mode  $\omega_S = \omega_a, \omega_I = \omega_b$  the scattering matrix takes the simpler form

$$\begin{bmatrix} \sqrt{G_0} & 0 & 0 & \sqrt{G_0 - 1}e^{-i\theta} \\ 0 & \sqrt{G_0} & \sqrt{G_0 - 1}e^{i\theta} & 0 \\ 0 & \sqrt{G_0 - 1}e^{-i\theta} & \sqrt{G_0} & 0 \\ \sqrt{G_0 - 1}e^{i\theta} & 0 & 0 & \sqrt{G_0} \end{bmatrix}, \quad (64)$$

where the zero-detuning, optimal amplifier power gain  $G_0$  is

$$G_0 = \left( \frac{1 + \rho_{ab}^2}{1 - \rho_{ab}^2} \right)^2. \quad (65)$$

It can be shown that the stability of the amplifier requires that  $\rho_{ab} < 1$ , i.e. there is a ceiling to the effective coupling between modes of the circuit, beyond which amplification turns into spontaneous parametric oscillations.

Note that the determinant of the scattering matrix is unity even in the fully general case. Also, it is important to realize that, quite generally, the scattering is not reciprocal. A wave going from port  $b$  to port  $a$  acquires a phase factor  $e^{-i\theta}$  from the drive which is conjugate to the phase factor  $e^{i\theta}$  accompanying the scattering from port  $a$  to port  $b$ .

We now turn to case ii) in which the scattering relations, while involve only one port, still are expressed as a  $4 \times 4$  matrix:

$$\begin{bmatrix} \mathbf{a}^{\text{out}}[+\omega_S] \\ \mathbf{a}^{\text{out}}[-\omega_S] \\ \mathbf{a}^{\text{out}}[+\omega_I] \\ \mathbf{a}^{\text{out}}[-\omega_I] \end{bmatrix} = \begin{bmatrix} r_{SS} & 0 & 0 & s_{SI} \\ 0 & r_{SS}^* & s_{SI}^* & 0 \\ 0 & s_{IS}^* & r_{II}^* & 0 \\ s_{IS} & 0 & 0 & r_{II} \end{bmatrix} \begin{bmatrix} \mathbf{a}^{\text{in}}[+\omega_S] \\ \mathbf{a}^{\text{in}}[-\omega_S] \\ \mathbf{a}^{\text{in}}[+\omega_I] \\ \mathbf{a}^{\text{in}}[-\omega_I] \end{bmatrix}. \quad (66)$$

Now the different frequencies are carried on the same port and are all in the vicinity of the single resonance of the unique mode. Nevertheless, the scattering coefficients are in the analytic continuation of the previous expressions, in which one simply sets  $\chi_b(\omega) = \chi_a(\omega)$ . A simplification occurs if the drive frequency is precisely tuned to twice the effective resonant frequency, i.e.  $\Omega_{aa} = 2\omega_a$ , in which case  $\chi_a(\omega_I) = \chi_a(\omega_S)^*$  and the subblock of the scattering matrix takes the form

$$\begin{bmatrix} \mathbf{a}^{\text{out}}[+\omega_S] \\ \mathbf{a}^{\text{out}}[-\omega_I] \end{bmatrix} = \frac{1}{D} \begin{bmatrix} |\chi_a^{-1}(\omega_S)|^2 + \rho_{aa}^2 & 2\rho_{aa}e^{-i\theta} \\ 2\rho_{aa}e^{i\theta} & |\chi_a^{-1}(\omega_S)|^2 + \rho_{aa}^2 \end{bmatrix} \begin{bmatrix} \mathbf{a}^{\text{in}}[+\omega_S] \\ \mathbf{a}^{\text{in}}[-\omega_I] \end{bmatrix}, \quad (67)$$

with  $D = [\chi_a^{-1}(\omega_S)]^2 - \rho_{aa}^2$  where  $\rho_{aa} = \frac{4g_{aa}}{\kappa_a}$ . We also introduce the in-phase and quadrature components of the incoming and outgoing waves:

$$\mathbf{a}_{\parallel,\perp}^{\text{in,out}}(\delta\omega) = \mathbf{a}^{\text{in,out}}[\omega_S] \pm e^{-i\theta} \mathbf{a}^{\text{in,out}}[-\omega_I], \quad (68)$$

where  $\delta\omega = \omega_S - \omega_a = \omega_a - \omega_I$ . The meaning of this transformation can be illustrated by the following consideration, which supposes  $\theta = 0$  for simplicity. Classically, if a signal is such that

$$y(t) = f(t) \cos(\omega_a t) + g(t) \sin(\omega_a t), \quad (69)$$

with in-phase and quadrature modulation components  $f(t)$  and  $g(t)$  slow compared to  $(\omega_a)^{-1}$ , then

$$y_{\parallel}(\delta\omega) = f(\delta\omega), \quad y_{\perp}(\delta\omega) = g(\delta\omega). \quad (70)$$

One can easily check that the effect of the angle  $\theta$  associated with the time dependence of the effective Hamiltonian is just to rotate the component signals in the Fresnel plane. In the representation where the in-phase and quadrature components form the basis signals, we find that the scattering matrix is diagonal

$$\mathbf{a}_{\parallel}^{\text{out}}(\delta\omega) = \frac{|\chi_a^{-1}(\omega_S)|^2 + 2\rho_{aa} + \rho_{aa}^2}{D} \mathbf{a}_{\parallel}^{\text{in}}(\delta\omega) = \Lambda_{\parallel}(\delta\omega) \mathbf{a}_{\parallel}^{\text{in}}, \quad (71)$$

$$\mathbf{a}_{\perp}^{\text{out}}(\delta\omega) = \frac{|\chi_a^{-1}(\omega_S)|^2 - 2\rho_{aa} + \rho_{aa}^2}{D} \mathbf{a}_{\perp}^{\text{in}}(\delta\omega) = \Lambda_{\perp}(\delta\omega) \mathbf{a}_{\perp}^{\text{in}}. \quad (72)$$

The property of the scattering matrix to have unity determinant imposes

$$G_{\parallel} G_{\perp} = 1. \quad (73)$$



where  $G_{\parallel,\perp} = |\Lambda_{\parallel,\perp}(\delta\omega)|^2$ . Thus, in this mode of operation of the degenerate parametric amplifier, one quadrature of the signal is amplified while the other is de-amplified. If the input signal consists only of vacuum fluctuations, the amplifier squeezes these fluctuations for one quadrature, making it less uncertain than the so-called standard quantum limit, which is associated to a standard deviation corresponding to the square root of a quarter of a photon (the half photon of the zero-point motion is split evenly between the two quadratures, and only one is squeezed) [12].

In the non-degenerate case (i) a more complex form of squeezing – two-mode squeezing – occurs in the four dimensional phase space of the quadratures of the two propagating signals incident on the circuit [12].

The non-degenerate parametric amplifier is usually employed as a sort of RF op-amp: the idler port is connected to a cold matched load emulating an infinite transmission line at zero-temperature and the device viewed from the signal port functions as a reflection amplifier operating in the phase preserving mode: for signals having a bandwidth small compared to that of the amplifier

$$\mathbf{a}^{\text{out}} = \sqrt{G} \left( \mathbf{a}^{\text{in}} + \sqrt{1 - \frac{1}{G}} \mathbf{b}^{\text{in}\dagger} \right). \quad (74)$$

The second term on the right of this last expression shows that quantum noise entering through the  $b$  port must necessarily be added to the amplified signal [2]. This added noise contribution amounts, in the large gain limit  $G \gg 1$  and for an idler port at zero temperature, to a half-photon at the signal frequency, referred to the input. It can be seen as an evil necessary to preserve the commutation relation

$$[\mathbf{a}^{\text{out}}, \mathbf{a}^{\text{out}\dagger}] = [\mathbf{a}^{\text{in}}, \mathbf{a}^{\text{in}\dagger}]. \quad (75)$$

More practically, the extra half-photon of noise can also be seen as a consequence of the Heisenberg Uncertainty Principle. A phase preserving amplifier processes equally both quadratures, which in quantum mechanics are non-commuting observables. Since the process of amplification is equivalent to measurement, the extra noise forbids that both quadratures are known precisely simultaneously, in accordance with the central principle of quantum mechanics. An amplifier functioning in this Heisenberg regime where the efficiency of the amplification process is only limited by irreducible quantum fluctuations is said to be quantum-limited.

## 5. Practical amplifier circuits based on Josephson junction circuits

We have introduced in the previous section the notion of effective, time-dependent quadratic Hamiltonians and shown how their generic form lead to the amplification of a quantum signal with a noise limited solely by the Heisenberg Uncertainty Principle. We now explain in this section how such quadratic forms can arise from a practical non-linear, damped and driven system based on Josephson tunnel junctions.

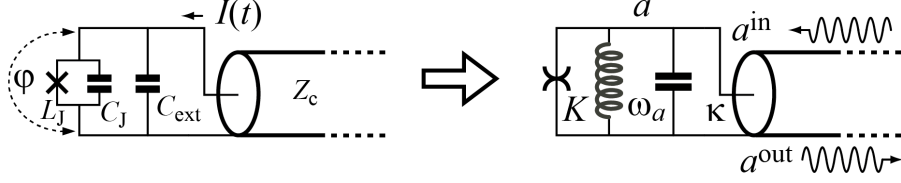


Figure 6: 1-mode, 1-port Josephson amplifier involving only the Josephson inductance. Left panel is schematic of Josephson tunnel junction, itself consisting of a Josephson tunnel element playing the role of non-linear inductance (cross,  $L_J$ ) and a junction capacitance  $C_J$ , in parallel with an external capacitance  $C_{\text{ext}}$  and a transmission line bringing in the current  $I(t)$ . The variable  $\varphi$  is the phase across the junction. On the right panel, simplified schematic based on an RWA treatment where the oscillator is reduced to its frequency  $\omega_a$  and damping rate  $\kappa$ , with the Josephson non-linearity manifesting itself as a simple Kerr component (opposing arcs symbols) characterized by the parameter  $K$ , the shift in frequency of the oscillator corresponding to 1 photon. The degree of freedom is described by the standing photon ladder operator  $\mathbf{a}$ .

### 5.1. Driven microwave oscillator whose inductance is a single Josephson element: Duffing-like dynamics

We first examine the simplest case of a 1-mode, 1-port circuit in which the inductance is just the Josephson element of superconducting tunnel junction (see Fig. 6) [13, 14]. The Hamiltonian of such systems is given by

$$\mathbf{H} = \mathbf{H}_{\text{circ}} - \frac{\hbar}{2e} \varphi \cdot \mathbf{I} + \mathbf{H}_{\text{env}}, \quad (76)$$

$$\mathbf{H}_{\text{circ}} = -E_J \cos \varphi + \frac{\mathbf{Q}^2}{2C_\Sigma}, \quad (77)$$

where  $E_J = (\frac{\hbar}{2e})^2 / L_J$  is the Josephson energy,  $C_\Sigma = C_J + C_{\text{ext}}$  is the total capacitance in parallel with the Josephson element,  $\varphi$  the gauge-invariant phase difference across the junction,  $\mathbf{Q}$  the charge conjugate to the phase  $[\varphi, \mathbf{Q}] = 2ei$ ,  $\mathbf{H}_{\text{env}}$  the Hamiltonian of the transmission line, including the pump arriving through this channel and  $\mathbf{I}$  the current operator belonging to the degrees of freedom of the line. The amplifier functions with  $\langle \varphi \rangle$  having excursions much less than  $\pi/2$  and the cosine function in the Hamiltonian can be expanded to 4<sup>th</sup> order only, with the  $\varphi^4$  term treated as a perturbation [15, 16]. Introducing the ladder operators of the single mode of the circuit

$$\varphi = \varphi_{\text{ZPF}} (\mathbf{a} + \mathbf{a}^\dagger) \quad (78)$$

and working in the framework of both an expansion in  $\varphi_{\text{ZPF}} = (2e^2/\hbar)^{1/2} (L_J/C_\Sigma)^{1/4}$  and RWA, the hamiltonian of the circuit simplifies to

$$\frac{\mathbf{H}_{\text{circ}}}{\hbar} = \tilde{\omega}_a \mathbf{a}^\dagger \mathbf{a} + \frac{K}{2} \mathbf{a}^\dagger \mathbf{a} (\mathbf{a}^\dagger \mathbf{a} - 1), \quad (79)$$

where, in the regime  $\varphi_{\text{ZPF}} \ll 1$ ,  $K = -e^2/(2\hbar C_\Sigma)$  and  $\tilde{\omega}_a = 1/\sqrt{L_J C_\Sigma} + K$ . The Quantum Langevin Equation applied to this system yields

$$\frac{d}{dt}\mathbf{a} = -i(\tilde{\omega}_a + K\mathbf{a}^\dagger\mathbf{a})\mathbf{a} - \frac{\kappa}{2}\mathbf{a} + \sqrt{\kappa}\mathbf{a}^{\text{in}}(t), \quad (80)$$

where  $\tilde{\omega}_a \gg \kappa_a \gg K$ . This last equation is the quantum version, in the RWA approximation, of the equation describing systems modeled by the Duffing equation. The classical Duffing oscillator obeys the equation

$$m\ddot{x} + \eta\dot{x} + m\omega_0^2x(1 + \mu x^2) = f_D \cos(\omega_D t) + f_P(t) \quad (81)$$

for the position variable  $x$  having mass  $m$ , small amplitude spring constant  $m\omega_0^2$ , friction coefficient  $\eta$  and driven at frequency  $\omega_D$ , which is close to the small amplitude resonant frequency  $\omega_0$ . A small probe force  $f_P(t)$  allows to study the displacement response of the system. Non-linearity of the oscillator corresponds here to the spring constant being dependent quadratically on position.

Here, for our amplifier,  $\kappa$  plays the role of the damping rate  $\eta/m$ , and  $K$  plays the role of  $\mu$ . Let us now suppose that, in addition to the signal to be processed, the  $a$  port also receives an intense drive tone described by a propagating coherent state with amplitude  $\alpha^{\text{in}}$  and frequency  $\Omega$ . We treat this drive by the change of variable

$$\mathbf{a}^{\text{in}}(t) = \alpha^{\text{in}}e^{-i\Omega t} + \delta\mathbf{a}^{\text{in}}(t), \quad (82)$$

$$\mathbf{a}(t) = \alpha e^{-i\Omega t} + \delta\mathbf{a}(t). \quad (83)$$

We aim to solve for the semi-classical amplitude  $\alpha$  from Eq. (80):

$$\frac{d\alpha}{dt} - i\Omega\alpha = -i\tilde{\omega}_a\alpha - iK|\alpha|^2\alpha - \frac{\kappa_a}{2}\alpha + \sqrt{\kappa_a}\alpha^{\text{in}}. \quad (84)$$

By treating the non-linear term as a perturbation, we obtain the self-consistent algebraic equation in steady state:

$$\alpha = \frac{i\sqrt{\kappa_a}\alpha^{\text{in}}}{(\Omega - \tilde{\omega}_a) + \frac{i\kappa_a}{2} - K|\alpha|^2}, \quad (85)$$

which in general yields for the c-number  $\alpha$  a complex value such

$$|\alpha - \alpha_0| \ll 1, \quad \alpha_0 = \frac{i\sqrt{\kappa_a}\alpha^{\text{in}}}{(\Omega - \tilde{\omega}_a) + \frac{i\kappa_a}{2} - 4K|\alpha^{\text{in}}|^2/\kappa_a}. \quad (86)$$

This value leads to the effective Hamiltonian for the degenerate parametric amplifier arising from the pumping of the Josephson junction

$$\frac{\mathbf{H}}{\hbar} = \omega_a\delta\mathbf{a}^\dagger\delta\mathbf{a} + \left[g_{aa}e^{i(\Omega_{aa}t+\theta)}(\delta\mathbf{a})^2 + h.c.\right] \quad (87)$$

with

$$\omega_a = \tilde{\omega}_a + 2K|\alpha|^2, \quad (88)$$

$$g_{aa}e^{i\theta} = K\alpha^{*2}, \quad (89)$$

$$\Omega_{aa} = 2\Omega. \quad (90)$$

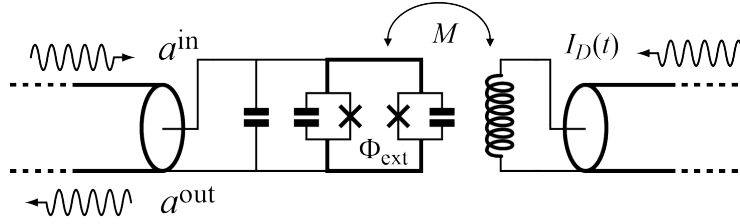


Figure 7: Parametrically driven oscillator based on the property of the Josephson inductance of a DC-SQUID (two Josephson junctions in parallel forming a loop, here represented by a thicker line) to be modulated by the variation of an external flux  $\Phi_{ext}$ . The modulation arises from an RF drive current  $I_D(t) = I_D^R \cos \Omega t$  in the primary of a transformer that creates through its mutual inductance  $M$  a sinusoidal flux variation in the loop of the DC-SQUID.

Eqs. (88), (90) put into light two drawbacks of this type of amplifier: the center frequency of the band of the amplifier shifts as the pump amplitude is increased and the pump tone needs to be at the center of the band for optimal amplification. The use of two pumps frequencies  $\Omega_1$  and  $\Omega_2$  such that  $\Omega_{aa} = \Omega_1 + \Omega_2$  facilitates the use of this parametric amplifier [17].

The device has noticeable gain when  $K |\alpha^{\text{in}}|^2 / \kappa_a^2$  is of order unity, implying that the number of pump photons in the oscillator is of order  $\kappa_a / K$ , a large number by hypothesis. This justifies our treatment of the pump drive as a c-number. Neglected terms such as the non-RWA term  $(\delta a)^3 e^{i\Omega t}$  have smaller factors and can themselves be treated as perturbations on top of the standard degenerate parametric amplifier formalism. It is worth noting that for this device, the pump tone and the signal tone must enter the circuit on the same port, which is inconvenient given the widely different amplitude levels of these two waves.

Amplifiers based on the same Duffing type of non-linearity can also be fabricated with two-port circuits containing arrays of Josephson junctions [18, 19].

### 5.2. A parametrically driven oscillator: the DC-SQUID driven by RF flux variation

Another class of Josephson circuit implementing parametric amplifiers at microwave frequencies is the RF-Flux-driven DC-SQUID (see Fig. 7).

It turns out that this parametric drive can be implemented in Josephson circuits by taking a DC-SQUID, which is formed by two nominally identical Josephson junctions in parallel and modulating at the RF pump frequency the flux  $\Phi_{ext}$  threading the superconducting loop between them (here the term DC refers to the circulating current in the loop due to an external bias flux). One exploits the functional form of the Josephson inductance of the DC-SQUID

$$L_J^{SQUID} = \frac{L_J}{\cos \left| \pi \frac{\Phi_{ext}}{\Phi_0} \right|}, \quad (91)$$

where  $\Phi_0 = h/2e$  is the flux quantum and  $L_J/2$  is the Josephson inductance of each individual junction. When

$$\Phi_{ext} = \frac{\Phi_0}{4} [1 + \varepsilon \cos(\Omega t)], \quad (92)$$

with  $\Omega$  close to the resonant frequency of the SQUID  $1/\sqrt{C_\Sigma L_J^{SQUID}}$  and  $\varepsilon \ll 1$ , one implements the parametrically driven harmonic oscillator with relative frequency modulation parameter  $\mu_r = \pi\varepsilon/4$ . This modulation is produced by a drive current  $I_D(t) = I_D^{RF} \cos(\Omega t)$  at the primary of the transformer coupling the transmission line of an RF pump to the flux of the SQUID (see Fig. 7). Classically, the parametrically driven harmonic oscillator obeys the equation

$$m\ddot{x} + \eta\dot{x} + m\omega_0^2 x [1 + \mu_r \cos(\Omega t)] = f_P(t). \quad (93)$$

In contrast with the Duffing oscillator above, this system is described by a fully linear, albeit time-dependent, equation. The drive, instead of appearing as a force coupled directly to position, now modulates the spring constant with a relative amplitude  $\mu_r$ . The system behaves as an amplifier when the argument of the cosine modulation term is such that the drive frequency  $\Omega$  is close to the resonant frequency  $\omega_0$ . In the weak damping limit  $\eta \ll m\omega_0$ , the quantum version of this oscillator is directly a one-port, one-mode system described by our degenerate amplifier Hamiltonian

$$\frac{\mathbf{H}}{\hbar} = \omega_a \mathbf{a}^\dagger \mathbf{a} + [g_{aa} e^{i\Omega_{aa} t} \mathbf{a}^2 + h.c.], \quad (94)$$

where

$$\Omega_{aa} = \Omega, \quad (95)$$

$$g_{aa} = \mu_r \omega_0 / 4. \quad (96)$$

Note that now the drive frequency needs to be near twice the resonance frequency of the amplified mode, unlike in the Duffing case, and it is thus easier to decouple the pump tone from the weak signal to be amplified. This type of amplifier has been implemented in several labs [20, 21, 22, 23].

### 5.3. 3-mode circuit employing the purely dispersive Josephson 3-wave mixer

We have just described the two ways in which a circuit involving one or two Josephson junctions can implement the degenerate parametric amplifier (case (ii) of last section). The non-degenerate parametric amplifier (case (i) of last section) can be implemented by a 3-mode, 3-port circuit employing four junctions forming the so-called Josephson ring modulator, a purely dispersive 3-wave mixer (see details in [24, 25, 26]).

Three microwave standing wave resonators are coupled by this last element and are described by the Hamiltonian

$$\frac{\mathbf{H}}{\hbar} = \omega_a \mathbf{a}^\dagger \mathbf{a} + \omega_b \mathbf{b}^\dagger \mathbf{b} + \omega_c \mathbf{c}^\dagger \mathbf{c} + g_3 (\mathbf{a} + \mathbf{a}^\dagger) (\mathbf{b} + \mathbf{b}^\dagger) (\mathbf{c} + \mathbf{c}^\dagger), \quad (97)$$

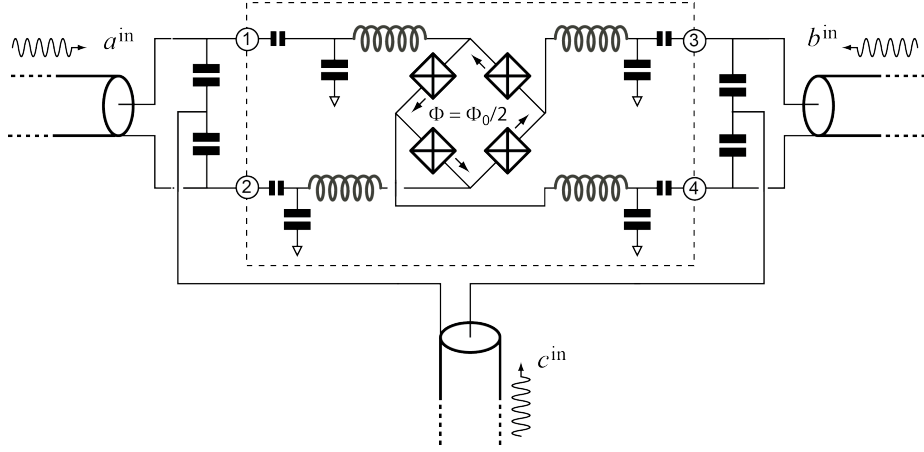


Figure 8: Schematic circuit of the purely dispersive 3-wave mixer (dashed line) involving three microwave modes, themselves coupled to three ports. The system functions as a non-degenerate parametric amplifier with mode  $a$  and  $b$  playing the role of the signal and idler, while mode  $c$  is used to couple in the pump tone. While there are in principle four modes coupled by the junctions (cross inside a square, denoting both the Josephson element and associated capacitance), the symmetry of the circuit when the junctions are identical, imposes that only three modes participate in the nonlinear interaction. A flux threading the ring of junctions induces a current (arrows) that replaces one of the four waves coupled by the junction.

together with their port coupling  $\kappa_a$ ,  $\kappa_b$  and  $\kappa_c$ . The frequency scales are such that

$$\omega_c \gg \omega_b > \omega_a > \kappa_c \gg \kappa_a \simeq \kappa_b \gg g_3. \quad (98)$$

The trilinear coupling term, treated as a perturbation, possesses the precious property that it does not, at the lowest order, offset the frequency of the quadratic terms when the modes are occupied by coherent signals, unlike the Kerr term above  $\frac{\kappa}{2} \mathbf{a}^\dagger \mathbf{a} (\mathbf{a}^\dagger \mathbf{a} - 1)$ . Other terms of higher order have been neglected in the Hamiltonian (97). They ensure that the system remains stable when the amplitudes become large, as the trilinear coupling renders by itself the Hamiltonian unstable. In the regime where the  $c$  mode is driven by a large coherent field  $\alpha_c^{\text{in}} e^{-i\Omega t}$ , we can neglect the fluctuating part of the corresponding operator. The previous Hamiltonian can be treated as

$$\frac{\mathbf{H}^{\text{eff}}}{\hbar} = \omega_a \mathbf{a}^\dagger \mathbf{a} + \omega_b \mathbf{b}^\dagger \mathbf{b} + 2g_{ab} (\mathbf{a} + \mathbf{a}^\dagger) (\mathbf{b} + \mathbf{b}^\dagger) \cos(\Omega_{ab}t + \theta), \quad (99)$$

where

$$g_{ab} \cos(\Omega_{ab}t + \theta) = g_3 \Re \left[ \frac{\sqrt{\kappa_c} \alpha_c^{\text{in}} e^{-i\Omega t}}{-i(\omega_{ab}^D - \omega_c) + \kappa_c} \right], \quad (100)$$

$$\Omega_{ab} = \Omega. \quad (101)$$

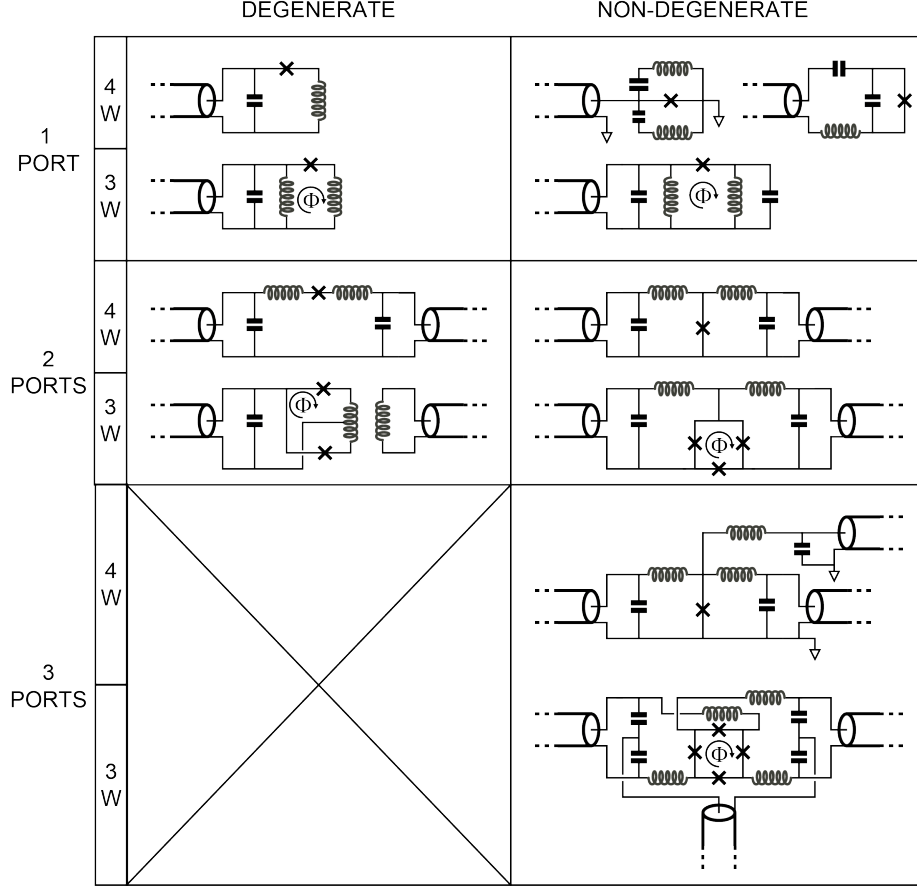


Figure 9: Minimalistic versions of the various Josephson circuits implementing parametric amplification of quantum signals. The circuits are classified according to the degenerate/non-degenerate character of the amplifying process (one or two standing modes). The four-wave (4W) or the three-wave (3W) labels characterize the mixing process for the signal and idler waves taking place in the Josephson junctions. In the three-wave process, the place of one of the four-waves incident on the junction is replaced by a DC current generated by the externally applied flux  $\Phi$ . We also distinguish circuits by the number of ports through which the signal, idler and the pump waves are delivered. In the upper left corner (minimal complexity), the three waves are approximately at the same frequency and arrive through the same port, whereas in the lower right corner (maximal complexity), the three waves are both spatially and spectrally separated. In the upper right corner, we have represented two implementations of the 1-port, 4-wave, non-degenerate parametric amplifier. In the circuit on the left-handside, the two modes share a common junction but are symmetrically coupled to the port, whereas on the right-handside, the two modes are gauge-coupled and are asymmetrically coupled to the port [27].

When one works within the framework of the Rotating Wave Approximation and  $\Omega_{ab} \simeq \omega_a + \omega_b$ , the fast rotating terms can be neglected and one recovers

the Hamiltonian of the generic non-degenerate parametric amplifier

$$\frac{\mathbf{H}^{\text{NDPA}}}{\hbar} = \omega_a \mathbf{a}^\dagger \mathbf{a} + \omega_b \mathbf{b}^\dagger \mathbf{b} + \left[ g_{ab} \mathbf{a} \mathbf{b} e^{i(\Omega_{ab}t + \theta)} + h.c. \right]. \quad (102)$$

## 6. Concluding Summary and Perspectives

In this short review, we have outlined the different ways in which Josephson circuits can implement the functions of parametric amplification. The key organizing concept is the effective quadratic time-dependent Hamiltonian which comes in two forms: degenerate and non-degenerate, depending on whether the signal and idler waves occupy the same physical degree of freedom or two separate ones. In Fig. 9, we summarize the different circuit configurations leading, on one hand, to the degenerate case and, on the other hand, to the non-degenerate case (left and right columns, respectively). The figure also classifies circuits depending on the number of access ports, the simpler case being that of 1-port carrying the signal, idler and pump waves (upper left panels), while the case in which the signal, idler and the pump waves are separated in both temporally and spatially is shown in the bottom right panel. The circuit complexity increases when going from the upper left corner of Fig. 9 to the lower right one.

This survey of amplifiers has not covered the following topics of current interest: dynamic range [26], directionality [28, 29, 19], efficiency and frequency-conversion. Lastly, recently several ideas have been proposed to make the amplifier avoid the gain-bandwidth compromise and the instability at the onset of parametric oscillation [30, 31]. These topics will be covered in an extended version of this review.

## Acknowledgments

The authors are grateful to Benjamin Huard, Michael Hatridge, Archana Kamal and Katrina Sliwa for valuable discussions in the preparation of this review. The authors thank Maxime Malnou for his critical reading of the manuscript. This work is supported by ARO under Grant No.W911NF-14-1-0011.

## References

- [1] M. H. Devoret, R. J. Schoelkopf, Superconducting Circuits for Quantum Information: An Outlook, *Science* 339 (6124) (2013) 1169–1174. doi:10.1126/science.1231930.  
URL <http://www.sciencemag.org/content/339/6124/1169.abstract>
- [2] C. M. Caves, Quantum limits on noise in linear amplifiers, *Phys. Rev. D* 26 (8) (1982) 1817–1839. doi:10.1103/PhysRevD.26.1817.  
URL <http://link.aps.org/doi/10.1103/PhysRevD.26.1817>



- [3] B. Yurke, P. G. Kaminsky, R. E. Miller, E. A. Whittaker, A. D. Smith, A. H. Silver, R. W. Simon, Observation of 4.2-K equilibrium-noise squeezing via a Josephson-parametric amplifier, *Phys. Rev. Lett.* 60 (9) (1988) 764–767. doi:10.1103/PhysRevLett.60.764. URL <http://link.aps.org/doi/10.1103/PhysRevLett.60.764>
- [4] B. Yurke, L. R. Corruccini, P. G. Kaminsky, L. W. Rupp, A. D. Smith, A. H. Silver, R. W. Simon, E. A. Whittaker, Observation of parametric amplification and deamplification in a Josephson parametric amplifier, *Phys. Rev. A* 39 (5) (1989) 2519–2533. doi:10.1103/PhysRevA.39.2519. URL <http://link.aps.org/doi/10.1103/PhysRevA.39.2519>
- [5] R. Vijay, D. H. Slichter, I. Siddiqi, Observation of Quantum Jumps in a Superconducting Artificial Atom, *Phys. Rev. Lett.* 106 (11) (2011) 110502. doi:10.1103/PhysRevLett.106.110502. URL <http://link.aps.org/doi/10.1103/PhysRevLett.106.110502>
- [6] M. Hatridge, S. Shankar, M. Mirrahimi, F. Schackert, K. Geerlings, T. Brecht, K. M. Sliwa, B. Abdo, L. Frunzio, S. M. Girvin, R. J. Schoelkopf, M. H. Devoret, Quantum Back-Action of an Individual Variable-Strength Measurement, *Science* 339 (6116) (2013) 178–181. doi:10.1126/science.1226897. URL <http://www.sciencemag.org/content/339/6116/178.abstract>
- [7] C. Gardiner, P. Zoller, *Quantum Noise: A Handbook of Markovian and Non-Markovian Quantum Stochastic Methods with Applications to Quantum Optics*, Springer Series in Synergetics, Springer, 2004. URL <https://books.google.com/books?id=a{ }xsT8oGhdgC>
- [8] D. F. Walls, G. J. Milburn, *Quantum Optics*, SpringerLink: Springer e-Books, Springer, 2008. URL <https://books.google.com/books?id=LiWsc3Nlf0kC>
- [9] S. Mallat, *A Wavelet Tour of Signal Processing*, Wavelet Tour of Signal Processing, Elsevier Science, 1999. URL <https://books.google.com/books?id=hbV0fWQntB8C>
- [10] A. S. Holevo, *Quantum Systems, Channels, Information: A Mathematical Introduction*, De Gruyter Studies in Mathematical Physics, De Gruyter, 2013. URL <https://books.google.com/books?id=zh{ }r0YaVI8C>
- [11] J.-M. Courty, F. Grassia, S. Reynaud, Quantum noise in ideal operational amplifiers, *EPL (Europhysics Letters)* 46 (1) (1999) 31. URL <http://stacks.iop.org/0295-5075/46/i=1/a=031>
- [12] P. D. Drummond, Z. Ficek, *Quantum Squeezing*, Springer Series on Atomic, Optical, and Plasma Physics, Springer Berlin Heidelberg, 2013. URL <https://books.google.com/books?id=VSzrCAAAQBAJ>

- [13] I. Siddiqi, R. Vijay, F. Pierre, C. M. Wilson, M. Metcalfe, C. Rigetti, L. Frunzio, M. H. Devoret, RF-Driven Josephson Bifurcation Amplifier for Quantum Measurement, *Phys. Rev. Lett.* 93 (20) (2004) 207002. doi:10.1103/PhysRevLett.93.207002.  
URL <http://link.aps.org/doi/10.1103/PhysRevLett.93.207002>
- [14] Josephson Bifurcation Amplifier: Amplifying quantum signals using a dynamical bifurcation, Yale University, 2008.
- [15] V. E. Manucharyan, E. Boaknin, M. Metcalfe, R. Vijay, I. Siddiqi, M. Devoret, Microwave bifurcation of a Josephson junction: Embedding-circuit requirements, *Phys. Rev. B* 76 (1) (2007) 14524. doi:10.1103/PhysRevB.76.014524.  
URL <http://link.aps.org/doi/10.1103/PhysRevB.76.014524>
- [16] S. E. Nigg, H. Paik, B. Vlastakis, G. Kirchmair, S. Shankar, L. Frunzio, M. H. Devoret, R. J. Schoelkopf, S. M. Girvin, Black-Box Superconducting Circuit Quantization, *Phys. Rev. Lett.* 108 (24) (2012) 240502. doi:10.1103/PhysRevLett.108.240502.  
URL <http://link.aps.org/doi/10.1103/PhysRevLett.108.240502>
- [17] A. Kamal, A. Marblestone, M. Devoret, Signal-to-pump back action and self-oscillation in double-pump Josephson parametric amplifier, *Phys. Rev. B* 79 (18) (2009) 184301. doi:10.1103/PhysRevB.79.184301.  
URL <http://link.aps.org/doi/10.1103/PhysRevB.79.184301>
- [18] M. A. Castellanos-Beltran, K. D. Irwin, G. C. Hilton, L. R. Vale, K. W. Lehnert, Amplification and squeezing of quantum noise with a tunable Josephson metamaterial, *Nat Phys* 4 (12) (2008) 929–931.  
URL <http://dx.doi.org/10.1038/nphys1090>
- [19] C. Macklin, K. O'Brien, D. Hover, M. E. Schwartz, V. Bolkhovskiy, X. Zhang, W. D. Oliver, I. Siddiqi, A nearquantum-limited Josephson traveling-wave parametric amplifier, *Science* 350 (6258) (2015) 307–310. doi:10.1126/science.aaa8525.  
URL <http://www.sciencemag.org/content/350/6258/307.abstract>
- [20] T. Yamamoto, K. Inomata, M. Watanabe, K. Matsuba, T. Miyazaki, W. D. Oliver, Y. Nakamura, J. S. Tsai, Flux-driven Josephson parametric amplifier, *Applied Physics Letters* 93 (4) (2008) –. doi:http://dx.doi.org/10.1063/1.2964182.  
URL <http://scitation.aip.org/content/aip/journal/apl/93/4/10.1063/1.2964182>
- [21] J. R. Johansson, G. Johansson, C. M. Wilson, F. Nori, Dynamical Casimir Effect in a Superconducting Coplanar Waveguide, *Phys. Rev. Lett.* 103 (14) (2009) 147003. doi:10.1103/PhysRevLett.103.147003.  
URL <http://link.aps.org/doi/10.1103/PhysRevLett.103.147003>

- [22] X. Zhou, V. Schmitt, P. Bertet, D. Vion, W. Wustmann, V. Shumeiko, D. Esteve, High-gain weakly nonlinear flux-modulated Josephson parametric amplifier using a SQUID array, *Phys. Rev. B* 89 (21) (2014) 214517. doi:[10.1103/PhysRevB.89.214517](https://doi.org/10.1103/PhysRevB.89.214517). URL <http://link.aps.org/doi/10.1103/PhysRevB.89.214517>
- [23] J. Y. Mutus, T. C. White, R. Barends, Y. Chen, Z. Chen, B. Chiaro, A. Dunsworth, E. Jeffrey, J. Kelly, A. Megrant, C. Neill, P. J. J. O Malley, P. Roushan, D. Sank, A. Vainsencher, J. Wenner, K. M. Sundqvist, A. N. Cleland, J. M. Martinis, Strong environmental coupling in a Josephson parametric amplifier, *Applied Physics Letters* 104 (26). doi:[http://dx.doi.org/10.1063/1.4886408](https://doi.org/10.1063/1.4886408). URL <http://scitation.aip.org/content/aip/journal/apl/104/26/10.1063/1.4886408>
- [24] N. Bergeal, R. Vijay, V. E. Manucharyan, I. Siddiqi, R. J. Schoelkopf, S. M. Girvin, M. H. Devoret, Analog information processing at the quantum limit with a Josephson ring modulator, *Nat Phys* 6 (4) (2010) 296–302. URL <http://dx.doi.org/10.1038/nphys1516>
- [25] N. Bergeal, F. Schackert, M. Metcalfe, R. Vijay, V. E. Manucharyan, L. Frunzio, D. E. Prober, R. J. Schoelkopf, S. M. Girvin, M. H. Devoret, Phase-preserving amplification near the quantum limit with a Josephson ring modulator, *Nature* 465 (7294) (2010) 64–68. URL <http://dx.doi.org/10.1038/nature09035>
- [26] B. Abdo, A. Kamal, M. Devoret, Nondegenerate three-wave mixing with the Josephson ring modulator, *Phys. Rev. B* 87 (1) (2013) 14508. doi:[10.1103/PhysRevB.87.014508](https://doi.org/10.1103/PhysRevB.87.014508). URL <http://link.aps.org/doi/10.1103/PhysRevB.87.014508>
- [27] T. Roy, S. Kundu, M. Chand, M. Vadiraj A., A. Ranadive, N. Nehra, M. P. Patankar, J. Aumentado, A. A. Clerk, R. Vijay, Broadband parametric amplification with impedance engineering: Beyond the gain-bandwidth product, *ArXiv e-prints* [arXiv:1510.03065](https://arxiv.org/abs/1510.03065).
- [28] A. Kamal, J. Clarke, M. H. Devoret, Noiseless non-reciprocity in a parametric active device, *Nat Phys* 7 (4) (2011) 311–315. URL <http://dx.doi.org/10.1038/nphys1893>
- [29] B. Abdo, K. Sliwa, S. Shankar, M. Hatridge, L. Frunzio, R. Schoelkopf, M. Devoret, Josephson Directional Amplifier for Quantum Measurement of Superconducting Circuits, *Phys. Rev. Lett.* 112 (16) (2014) 167701. doi:[10.1103/PhysRevLett.112.167701](https://doi.org/10.1103/PhysRevLett.112.167701). URL <http://link.aps.org/doi/10.1103/PhysRevLett.112.167701>
- [30] A. Metelmann, A. A. Clerk, Quantum-Limited Amplification via Reservoir Engineering, *Phys. Rev. Lett.* 112 (13) (2014) 133904. doi:[10.1103/PhysRevLett.112.133904](https://doi.org/10.1103/PhysRevLett.112.133904)

PhysRevLett.112.133904.

URL <http://link.aps.org/doi/10.1103/PhysRevLett.112.133904>

- [31] L. Ranzani, J. Aumentado, Graph-based analysis of nonreciprocity in coupled-mode systems, New Journal of Physics 17 (2) (2015) 23024.

URL <http://stacks.iop.org/1367-2630/17/i=2/a=023024>